Available online at www.sciencedirect.com

ScienceDirect

Geochimica et Cosmochimica Acta 72 (2008) 574–589

Geochimica et Cosmochimica Acta

www.elsevier.com/locate/gca

Metal–silicate partitioning and constraints on core composition and oxygen fugacity during Earth accretion

Alexandre Corgne [a,b,*], Shantanu Keshav [a,c], Bernard J. Wood [b], William F. McDonough [d], Yingwei Fei [a]

[a] *Geophysical Laboratory, Carnegie Institution of Washington, Washington, DC 20015, USA*
[b] *GEMOC, Macquarie University, North Ryde, NSW 2109, Australia*
[c] *Bayerisches Geoinstitut, Universität Bayreuth, D-95440 Bayreuth, Germany*
[d] *Department of Geology, University of Maryland, College Park, MD 20742, USA*

Received 17 April 2007; accepted in revised form 5 October 2007; available online 13 October 2007

Abstract

We present the results of new partitioning experiments between metal and silicate melts for a series of elements normally regarded as refractory lithophile and moderately siderophile and volatile. These include Si, Ti, Ni, Cr, Mn, Ga, Nb, Ta, Cu and Zn. Our new data obtained at 3.6 and 7.7 GPa and between 2123 and 2473 K are combined with literature data to parameterize the individual effects of oxygen fugacity, temperature, pressure and composition on partitioning. We find that Ni, Cu and Zn become less siderophile with increasing temperature. In contrast, Mn, Cr, Si, Ta, Nb, Ga and Ti become more siderophile with increasing temperature, with the highly charged cations (Nb, Ta, Si and Ti) being the most sensitive to variations of temperature. We also find that Ni, Cr, Nb, Ta and Ga become less siderophile with increasing pressure, while Mn becomes more siderophile with increasing pressure. Pressure effects on the partitioning of Si, Ti, Cu and Zn appear to be negligible, as are the effects of silicate melt composition on the partitioning of divalent cations. From the derived parameterization, we predict that the silicate Earth abundances of the elements mentioned above are best explained if core formation in a magma ocean took place under increasing conditions of oxygen fugacity, starting from moderately reduced conditions and finishing at the current mantle–core equilibrium value.

1. INTRODUCTION

High-pressure metal–silicate partitioning experiments demonstrate that the mantle contents of some moderately siderophile elements (Ni, Co, P, W, Mo, V) are consistent with core–mantle equilibration at high pressures and high temperatures (e.g. Walker et al., 1993; Hillgren et al., 1994; Thibault and Walter, 1995; Li and Agee, 1996; Righter and Drake, 1997; Chabot and Agee, 2003; Wade and Wood, 2005). This conclusion is one of the bases for the magma ocean theory, in which molten core materials segregate through a largely molten silicate mantle. To constrain further such theory, one should ask whether these conditions of core formation are consistent with the mantle contents of other elements. For example, the mantle contents of highly siderophile elements (Au, Re, PGEs) may be too elevated to be explained by simple core–mantle equilibration in a magma ocean, and may, instead, indicate the accretion of a late veneer of chondritic material to the mantle after core formation (e.g. Holzheid et al., 2000; Ertel et al., 2006). However, the 'late veneer' model is under debate with other reports reaching opposite conclusions (Righter and Drake, 1997; Danielson et al., 2005; Cottrell and Walker, 2006). In addition to pressure and temperature, composition is a key factor that can affect element distribution during core formation. In particular, the degree of oxidation of the planetary building materials, which depends on composition, has been shown to be a critical

---

[*] Corresponding author. Fax: +61 2 9850 6904.
E-mail address: acorgne@els.mq.edu.au (A. Corgne).

0016-7037/$ - see front matter © 2007 Elsevier Ltd. All rights reserved.
doi:10.1016/j.gca.2007.10.006

parameter. Since models have often called for an increase of oxygen fugacity (fo_2, a measure of the oxidation state) during planetary accretion and core formation (e.g. Wanke, 1981; O'Neill, 1991; Wade and Wood, 2005), it is important to constrain the effect of oxygen fugacity on partitioning.

Here, we report new metal–silicate partitioning data at 3.6 and 7.7 GPa and between 2123 and 2473 K for elements normally regarded as moderately volatile (Mn, Cr, Ga, Cu and Zn) and refractory lithophile (Nb, Ta, Ti, Sc, Lu, Hf, U, Th, Sm and Nd). The latter are generally assumed to be present entirely in the silicate Earth, whereas a more significant proportion of the former probably entered the core. Of the moderately volatile elements Ga is typically siderophile (it is a classifying element for iron meteorites), while Mn, Cr and Zn are both oxyphile and siderophile, depending on oxygen fugacity, and Cu has chalcophile, siderophile and oxyphile tendencies. Mantle depletions of all of these latter elements relative to their abundance in CI chondrites may also indicate loss by volatilization (or incomplete condensation) prior to and during planetary accretion (e.g. Walter et al., 2000).

This contribution builds upon and tests further the model of Wade and Wood (2005) for a progressively oxidizing Earth during accretion. Our new data are combined with literature data to parameterize, following the thermodynamic methodology described by Wade and Wood (2005), the individual effects of composition, pressure, temperature and fo_2 on partitioning and provide some answers to the following questions:

1. What is the range of composition–pressure–temperature–fo_2 conditions under which core formation in a magma ocean is compatible with the known mantle contents of these elements?
2. What constraints do these conditions (particularly oxygen fugacity) place on the trace element budget of the core?
3. Are the depletions of Ga, Cr, Zn and Mn in the mantle due to their volatility or, alternatively, a combination of this and sequestration into the core?

2. METHODS

Partitioning experiments between metal and silicate melts were performed on two synthetic compositions prepared from high-purity oxides, carbonates and metals. Following the work of Thibault and Walter (1995), the relative proportions of Si, Al, Ca, Mg, Fe and Ni in the first composition (SM-1) were chosen to resemble that of CI-chondrite (Wasson and Kallemeyn, 1988). The relative abundances of metal Fe and Fe_2O_3 were such that, after melting, the amount of FeO in the silicate melt is close to primitive mantle value. This imposes that SM-1 is largely depleted in O when compared with CI-chondrite (32 and 41 wt%, respectively). To assess the effect of oxygen fugacity on partitioning, a more reduced starting material (SM-2) was also prepared. Compared to SM-1, SM-2 is enriched in Si and Fe and depleted in O (Table 1), and resembles more E-chondrite composition (Wasson and Kallemeyn, 1988). To prepare the two starting materials, the required proportions of dried SiO_2, Al_2O_3, MgO and CaO (as $CaCO_3$) were first mixed, then slowly decarbonated in air from 600 to 1000 °C. Minor and trace elements were added as AAS solutions (~3000 ppm each of Nb, Ta, Ga, Sc, U, Th, Lu, Hf, Sm and Nd) and high-purity oxides (~6000 ppm Ti, ~7000 ppm Cr, ~2500 ppm Mn) to the silicate mixture. This mixture was then denitrified in air at 800 °C for 2 h. The appropriate amounts of Ni (~1.6 wt%), Fe, Fe_2O_3 and $Fe_{83}Si_{17}$ were then added to split portions of the silicate mixture. In SM-1, Fe was added as Fe metal (~26 wt%) and Fe_2O_3 (~4.4 wt%), while, in SM-2, Fe was added as Fe metal (~10.6 wt%) and $Fe_{83}Si_{17}$ (~21.4 wt%). The starting powders were homogenized under ethanol, finally dried at 100 °C for 24 h, and stored in a desiccator to minimize water content. Final (nominal) concentrations of the two starting compositions are reported in Table 1.

Table 1
Nominal compositions of the starting materials (in wt%)

	SM-1	SM-2
O	32.02	30.23
Mg	15.28	15.04
Fe	28.77	29.22
Si	16.56	18.25
Al	1.36	1.34
Ca	1.46	1.43
Ti	0.39	0.39
Ni	1.58	1.56
Mn	0.16	0.16
Cr	0.46	0.45
Ga	0.20	0.19
Nb	0.20	0.19
Ta	0.20	0.19
Sc	0.20	0.19
Nd	0.20	0.19
Sm	0.20	0.19
Lu	0.20	0.19
Hf	0.20	0.19
Th	0.20	0.19
U	0.20	0.19
Total	100.00	100.00

Experiments were carried out at 3.6 ± 0.2 and 7.7 ± 0.3 GPa and between 2123 and 2473 K using multi-anvil presses at the Geophysical Laboratory. We followed the same experimental procedure as Corgne et al. (2007). The reader is referred to that study and Table 2 for additional experimental details. As done in previous metal–silicate partitioning studies (e.g. Thibault and Walter, 1995; Corgne et al., 2007), we kept run durations relatively short to minimize metal infiltration into the graphite capsules. Furthermore, Thibault and Walter (1995) have shown that run durations as short as a few tens of seconds were sufficient to approach chemical equilibrium in this type of experiment. This point is discussed further in Section 3.2. We were unable to collect partitioning data from multi-anvil runs performed at pressures above 7.7 GPa. As observed by Thibault and Walter (1995), capsule transformation to diamond at these conditions induced rapid liquid metal dispersion within the capsule. Metal blobs remaining in

Table 2
Experimental details[a]

Run	Composition	*P* (GPa)	*T* (K)	*t* (s)	ΔIW[b]	ΔIW[c]	*nbo*/*t*[d]
PL-169	SM-1	3.6	2123	100	−0.8	−2.0	2.1
PL-185	SM-1	3.6	2273	100	−0.9	−2.0	2.1
PR-369	SM-1	3.6	2473	100	−1.1	−2.1	2.1
PR-373	SM-1	7.7	2273	100	−0.6	−1.9	2.2
PR-376	SM-2	3.6	2273	20	−3.2	−4.4	1.8
PR-383	SM-2	3.6	2273	100	−3.1	−4.4	1.7
PR-375	SM-2	3.6	2273	600	−3.0	−4.2	1.7
PR-368	SM-2	3.6	2473	100	−3.1	−4.4	1.8
PR-365	SM-2	7.7	2273	110	−3.2	−4.4	1.7

[a] Notations: *P*, pressure; *T*, temperature; *t*, run duration.

[b] Oxygen fugacity relative to the iron–wüstite buffer calculated using $\gamma_{\mathrm{FeO}}^{\mathrm{silicate}} = 3$ and $\gamma_{\mathrm{Fe}}^{\mathrm{metal}} = 0.8$ (see text for details).

[c] Oxygen fugacity relative to the iron–wüstite buffer calculated assuming ideal mixing behaviour (for comparison).

[d] *nbo*/*t*: molar ratio of non-bridging oxygen to tetrahedrally coordinated cations calculated assuming all Fe as Fe^{2+}.

contact with silicate melt were unfortunately too small (<10 μm) to measure their trace element contents.

Major and minor element contents of the experimental charges were measured using the 5-spectrometer JEOL 8900 electron probe micro-analyzer (EPMA) at the Geophysical Laboratory. We used a series of silicate, oxide and metal standards and conditions of 30 nA beam current and 15 kV accelerating voltage. Analyses were made with a defocused beam (10–30 μm diameter) to average the compositions of the fine-grained quench phases that composed metal and silicate phases. Analyses were reduced using a ZAF correction routine. After removal of the carbon coating, carbon contents in metal were measured using a PC-2 crystal on the CAMECA SX100 microprobe at GEMOC. A calibration curve for the C Kα line intensity was established using synthetic standards containing 0.0, 0.39, 0.57, 0.87, 5.3 wt% carbon (NIST steel standards and two in-house standards) and a natural cohenite from the Canyon Diablo meteorite (6.7 wt% carbon). The following relation was derived: C Kα line intensity (cps/s/nA) = 7.0 ∗ C content (wt%) + 3.3. The systematic analysis of standards after each unknown sample confirmed the reproducibility of the calibration. Analytical conditions were 15 kV accelerating voltage and 20 nA beam current for a beam diameter of 5–10 μm.

Minor and trace element contents were measured using LA-ICPMS microprobes at the University of Maryland (UMD) and at GEMOC. These analyses were performed with Nd:YAG New Wave Research laser systems (UMD: 213 nm wavelength, 6–10 Hz frequency, 4–6 J/cm^2 power; GEMOC: 266 nm, 5 Hz, 5.5 J/cm^2) coupled to magnetic sector ICP mass spectrometer (Finnigan Element 2, UMD) or a quadrupole mass spectrometer (Agilent 7500S, GEMOC). The ablation cells were flushed with He to enhance sensitivity. Laser ablation was operated in spot and line sampling mode with a beam diameter between 30 and 100 μm depending on phase morphology. Background gas blanks were measured on all masses for 30–60 s before laser ablation. Total laser firing time ranged between 30 and 120 s. The reference NIST 610 glass was used as calibration standard for both metal and silicate phases. Selected time-resolved spectra were processed using a modified version of LAMTRACE (UMD) and GLITTER (GEMOC) to apply background subtraction and calculate absolute element abundances. Variations in ablation yields were corrected by reference to Mn and Ni concentrations measured by EPMA, respectively, for the silicate and the metal. Minimum detection limits are calculated on the basis of three standard deviations above the background count rate (99% confidence). The use of a platinum cone for the ICPMS at GEMOC rather than the more common Ni cone (as used in UMD) allowed us to measure low Ni concentrations in the silicate melts, with detection limits reaching sub-ppm levels. Repeat analyses of the NIST 610 standard show that the analytical uncertainties are better than ±3% for all measured elements. Accuracy was assessed by comparing observed and published contents of secondary silicate and steel standards (BCR-2G, NIST 661). Available observed/published content ratios show that accuracy is within ±10% or better for all elements except for Nb (15%) and Ta (18%) in metal. Duplicate analyses usually show excellent agreement between data from the EPMA and both LA-ICPMS microprobes. However, for a reason that remains unclear to us, Nb and Ta measurements at UMD were inconsistent with results from the other two techniques and mass balance considerations. These UMD data were not used.

3. RESULTS

3.1. Phase morphology and major element composition

All samples contain blebs of molten alloy up to 200 μm across and surrounded by quench silicate melt (Fig. 1), the latter constituting approximately 70% of the experimental charge. EPMA profiles and LA-ICPMS time-resolved spectra across the metal alloy and silicate phases suggest that both phases are compositionally homogeneous, hence that equilibrium conditions are approached. The main compositional features of the metal and silicate phases are as follows. At relatively low oxygen fugacity (SM-2 composition), the alloy contains about 82 wt% Fe, 5 wt% Ni, 10 wt% Si, 1–2 wt% C and significant amounts of Cr, Mn, Nb, Ta, Ga and Ti (Table 3). In contrast, at higher oxygen fugacity (SM-1), the alloy is essentially made of about 90 wt% Fe, 5 wt% Ni and 5 wt% C. At low oxygen fugacity, the silicate melt contains significantly less Fe,

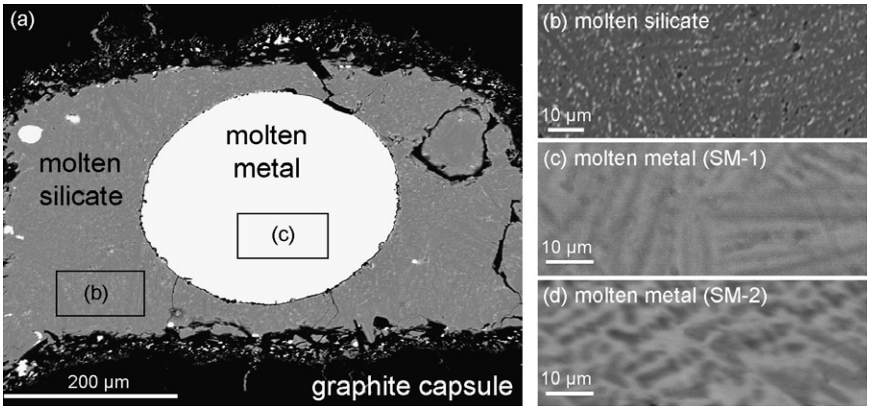

Fig. 1. Back-scattered electron images of run products showing typical phase morphologies and dimensions. (a) Products of run PL185 (starting composition SM-1) with magnified views of (b) the molten silicate and (c) the molten metal. (d) Detailed view of the quench texture of the molten metal in run PR365 (starting composition SM-2). As shown in these images, metal and silicate liquids did not quench to a single phase. The silicate melt, which developed similar texture with both SM-1 and SM-2 starting compositions upon quenching, is composed of a mixture of dendritic quench crystals and possibly interstitial glass (see b). Two quench textures are observed for the metal depending on the starting compositions. In runs performed using SM-2, the metal quenched as two phases, one (light grey) being slightly more enriched in Si and Ni and slightly more depleted in Cr and C than the other one (dark grey) (see d). Metal liquids in runs performed using SM-1 exhibit a more subtle quench texture than in runs using SM-2, with dendrites of Fe-rich alloys only visible at very high contrast (see c).

Table 3
Average metal compositions

	PL-169	PL-185	PR-369	PR-373	PR-376	PR-383	PR-375	PR-368	PR-365
EPMA	$N = 9$[a]	$N = 11$	$N = 10$	$N = 10$	$N = 10$	$N = 13$	$N = 10$	$N = 11$	$N = 12$
Fe (wt%)	89.72 (19)[b]	89.52 (6)	88.45 (28)	87.28 (22)	82.19 (30)	81.80 (13)	82.24 (22)	82.45 (15)	82.79 (61)
Ni	5.66 (10)	5.21 (17)	3.77 (8)	5.22 (10)	4.63 (9)	5.14 (5)	4.25 (6)	4.38 (8)	4.25 (24)
Si	0.036 (2)	0.036 (16)	0.039 (2)	0.025 (1)	9.03 (20)	9.54 (12)	9.92 (21)	9.70 (22)	9.25 (29)
Mn	<0.01[c]	<0.01	0.020 (2)	<0.01	0.22 (2)	0.22 (1)	0.23 (1)	0.24 (1)	0.27 (4)
Cr	0.26 (3)	0.44 (2)	0.66 (2)	0.42 (2)	1.11 (5)	1.14 (3)	1.09 (4)	1.09 (5)	1.20 (7)
Ti	<0.006	<0.006	<0.006	<0.006	0.11 (1)	0.10 (1)	0.09 (1)	0.09 (1)	0.07 (1)
Ga	0.40 (2)	0.35 (2)	0.40 (3)	0.27 (2)	0.45 (1)	0.48 (1)	0.50 (2)	0.47 (1)	0.43 (2)
Nb	0.013 (6)	0.047 (18)	0.12 (1)	0.043 (16)	0.50 (6)	0.57 (8)	0.31 (3)	0.43 (5)	0.41 (4)
Ta	<0.028	<0.028	<0.028	<0.028	0.39 (5)	0.38 (5)	0.21 (4)	0.34 (5)	0.32 (4)
O	0.21 (1)	0.18 (1)	0.18 (1)	0.17 (1)	0.22 (4)	0.21 (1)	0.19 (1)	0.22 (1)	0.21 (1)
C	5.0 (5)	4.7 (2)	4.3 (4)	6.1 (3)	1.7 (5)	1.6 (3)	1.9 (4)	2.0 (1)	1.4 (5)
Total	101.2	100.4	99.3	99.5	100.5	101.2	101.2	101.4	100.6
LA-ICPMS[d]	$N = 4$	$N = 3$	$N = 4$	$N = 4$	$N = 4$	$N = 4$	$N = 4$	$N = 3$	$N = 3$
Ti (ppm)	<10	<10	<10	<10	1273 (58)	1199 (61)	1265(67)	1452 (91)	957 (56)
Cr	2714 (80)	3970 (128)	6247 (205)	3631 (122)	11635 (378)	11310 (366)	11403 (371)	11421 (375)	13619 (650)
Mn	35 (1)	88 (3)	174 (6)	79 (3)	2272 (74)	2289 (76)	2589 (87)	2739 (93)	2815 (97)
Ga	4036 (157)	4073 (135)	4197 (143)	2867 (101)	4970 (175)	5106(183)	5450 (199)	5080 (189)	5016 (191)
Nb	76 (2)	449(15)	1043 (35)	296 (10)	4351 (203)	4854 (238)	2955(150)	4441 (234)	4140 (228)
Ta	24 (1)	40 (1)	58 (2)	51 (2)	3678 (194)	3689 (206)	2213 (128)	3714 (224)	4063 (256)
Cu	69 (3)	92 (3)	14 (1)	59 (2)	336 (11)	248 (8)	150 (5)	239 (8)	329 (11)
Zn	14 (1)	5.3 (1)	20 (1)	9 (1)	54 (2)	58 (2)	55 (2)	48 (2)	41(2)

[a] Number of EPMA and LA-ICPMS analyses.

[b] Values in parentheses are two standard errors for EPMA and one standard error for LA-ICPMS in terms of least digits cited.

[c] Contents below detection limit.

[d] LA-ICPMS data presented here are from measurements made at GEMOC. LA-ICPMS measurements made at UMD show that Sc, Nd, Sm, Lu, Hf, Th and U have concentrations in the alloy below detection limits (<ppm level).

Ni, Cr, Ga, Nb and Ta, but it is slightly more enriched in O and Si. A complete summary of element concentrations of alloy and silicate phases is given in Tables 3 and 4, respectively. Resulting molar metal–silicate partition coefficients (D^*_M, with D^*_M = mol% concentration of M in liquid metal/mol% concentration of $MO_{n/2}$ in silicate melt) are given in Table 5. Molar partition coefficients rather than weight partition coefficients were used in this study to characterize element partitioning between metal and silicate.

3.2. Time series

Experiments were performed at 3.6 GPa and 2273 K on the SM-2 starting composition to test the observations

Table 4
Average silicate compositions

	PL-169	PL-185	PR-369	PR-373	PR-376	PR-383	PR-375	PR-368	PR-365
EPMA	$N = 14$[a]	$N = 17$	$N = 13$	$N = 16$	$N = 19$	$N = 14$	$N = 20$	$N = 14$	$N = 20$
O (wt%)	43.46 (84)[a]	43.38 (40)	43.53 (149)	42.74 (73)	45.33 (12)	45.95 (15)	45.54 (23)	45.41 (23)	45.76 (75)
Mg	19.02 (22)	18.91 (18)	20.38 (69)	18.75 (22)	20.18 (4)	20.57 (2)	20.26 (5)	20.67 (9)	20.23 (21)
Fe	8.15 14)	7.96 (12)	6.50 (34)	8.37 (6)	0.50 (1)	0.52 (1)	0.62 (1)	0.53 (4)	0.51 (1)
Al	1.78 (5)	1.63 (5)	3.36 (5)	1.74 (3)	1.90 (1)	1.74 (1)	2.83 (2)	1.91 (2)	1.87 (1)
Si	22.22 (42)	22.43 (9)	20.91 (53)	21.64 (33)	25.13 (5)	25.79 (8)	24.61 (12)	24.89 (8)	25.65 (45)
Ca	1.63 (12)	1.72 (8)	1.46 (58)	1.97 (18)	2.02 (1)	1.62 (2)	1.82 (2)	2.04 (1)	1.63 (10)
Mn	0.24 (1)	0.25 (1)	0.23 (1)	0.22 (1)	0.25 (1)	0.24 (1)	0.21 (1)	0.22 (1)	0.25 (1)
Sc	0.26 (4)	0.23 (1)	0.23 (1)	0.24 (2)	0.30 (2)	0.25 (2)	0.28 (2)	0.29 (4)	0.26 (2)
Ti	0.55 (1)	0.44 (1)	0.45 (1)	0.52 (4)	0.51 (1)	0.46 (1)	0.51 (1)	0.51 (1)	0.54 (2)
Cr	0.45 (2)	0.46 (3)	0.32 (1)	0.42 (3)	0.06 (1)	0.06 (1)	0.06 (1)	0.06 (1)	0.07 (1)
Nb	0.20 (4)	0.20 (2)	0.11 (1)	0.23 (4)	<0.02[a]	<0.02	<0.02	<0.02	<0.02
Nd	0.21 (3)	0.17 (4)	0.17 (4)	0.17 (2)	0.26 (2)	0.21 (2)	0.20 (2)	0.25 (3)	0.23 (3)
Sm	0.18 (4)	0.18 (5)	0.17 (3)	0.19 (1)	0.26 (2)	0.20 (1)	0.24 (1)	0.27 (3)	0.17 (1)
Lu	0.16 (2)	0.20 (2)	0.17 (2)	0.17 (1)	0.23 (1)	0.19 (4)	0.22 (4)	0.26 (2)	0.20 (1)
Hf	0.20 (2)	0.19 (1)	0.19 (1)	0.20 (3)	0.24 (1)	0.19 (1)	0.26 (1)	0.25 (3)	0.24 (5)
Ta	0.22 (4)	0.20 (3)	0.17 (3)	0.21 (5)	<0.06	<0.06	<0.06	<0.06	<0.06
Th	0.18 (2)	0.19 (5)	0.19 (6)	0.15 (1)	0.24 (2)	0.19 (1)	0.21 (1)	0.27 (3)	0.20 (2)
Total	99.09	98.74	98.53	97.92	97.40	98.18	97.87	97.83	97.81
LA-ICPMS[b]	$N = 6/3$[c]	$N = 6/3$	$N = 6/3$	$N = 6/3$	$N = 6/2$	$N = 4/3$	$N = 4/3$	$N = 4/3$	$N = 5/3$
Mg (wt%)	18.79 (56)	19.16 (95)	21.45 (186)	17.12 (99)	18.97 (50)	19.91 (39)	19.50 (92)	18.80 (45)	19.15 (109)
Fe	7.92 (40)	7.04 (44)	6.15 (68)	6.82 (52)	0.38 (2)	0.49 (2)	0.61 (5)	0.49 (2)	0.49 (5)
Al	1.93 (9)	1.86 (5)	3.81 (17)	1.74 (4)	1.85 (7)	1.83 (5)	2.97 (20)	1.89 (7)	1.88 (16)
Si	25.11 (65)	27.44 (78)	25.36 (117)	22.05 (58)	26.14 (65)	28.19 (52)	26.42 (115)	24.91 (54)	28.07 (143)
Ca	1.77 (7)	1.57 (4)	1.59 (7)	1.80 (5)	1.94 (6)	1.68 (4)	1.90 (11)	2.00 (6)	1.69 (12)
Sc (ppm)	1991 (75)	2254 (69)	1922 (42)	2009 (34)	2615 (34)	2260 (81)	2373 (20)	2260 (94)	2212 (136)
Ti	5739 (258)	5140 (150)	5068 (244)	5322 (151)	5221 (188)	5101 (141)	5448 (367)	5160 (177)	5565 (470)
Cr	4572 (132)	5191 (146)	2943 (13)	3584 (96)	666 (18)	701 (14)	685 (32)	627 (15)	729 (41)
Ni	66 (2)	79 (2)	152 (8)	193 (6)	8.3 (3)	12.1 (3)	21 (1)	15.0 (4)	8.4 (6)
Cu	3.0 (1)	4.3 (1)	1.2 (1)	3.7 (1)	3.6 (1)	2.5 (11)	2.7 (2)	8.2 (2)	3.3 (2)
Zn	10.1 (4)	10.8 (4)	10.3 (6)	9.3 (3)	3.8 (2)	4.8 (2)	5.8 (4)	8.4 (2)	5.5 (5)
Ga	1001 (31)	1216 (33)	998 (44)	1228 (31)	73 (2)	101 (2)	133 (7)	101 (2)	70 (4)
Nb	2462 (107)	2068 (57)	1613 (73)	2267 (59)	20 (1)	25 (1)	32 (2)	24 (1)	33 (3)
Nd	1719 (232)	1848 (51)	1606 (28)	2002 (53)	2502 (112)	1995 (55)	2232 (11)	2357 (25)	1878 (115)
Sm	1714 (220)	1906 (32)	1605 (30)	2019 (30)	2478 (114)	2008 (66)	2242 (39)	2313 (37)	1883 (124)
Lu	1711 (150)	2239 (63)	1596 (25)	1919 (47)	2527 (85)	2097 (106)	2251 (32)	2242 (62)	2023 (155)
Hf	1714 (128)	2162 (63)	1587 (17)	1781 (49)	2496 (88)	2100 (101)	2228 (21)	2177 (60)	2051 (146)
Ta	2563 (126)	2135 (58)	2130 (94)	2511 (63)	321 (13)	341 (10)	363 (27)	300 (11)	414 (39)
Th	1667 (189)	1920 (15)	1554 (20)	1720 (33)	2679 (123)	1956 (83)	2227 (67)	2192 (108)	1869 (145)
U	1695 (229)	1763 (90)	1714 (30)	1800 (42)	2670 (98)	1967 (22)	2264 (109)	2227 (250)	2032 (140)

[a] Same notations as in Table 3.

[b] LA-ICPMS measurements for Sc, Nd, Sm, Lu, Hf, Th and U were made at UMD. LA-ICPMS data for Mg, Fe, Al, Si, Ca, Ti, Cr, Ni, Cu, Zn, Ga, Nb and Ta were obtained at GEMOC.

[c] Number of LA-ICPMS analyses ($N = a/b$, where a and b are the number of analyses made at UMD and GEMOC, respectively).

Table 5
Metal–silicate molar partition coefficients[a]

	PL-169	PL-185	PR-369	PR-373	PR-376	PR-383	PR-375	PR-368	PR-365
Fe	9.6 (2)[b]	9.9 (2)	12.5 (7)	8.8 (1)	150 (4)	144 (3)	120 (3)	139 (11)	148 (4)
Mn	0.013 (1)	0.030 (3)	0.069 (7)	0.030 (4)	0.84 (4)	0.86 (4)	1.10 (6)	1.12 (5)	1.05 (7)
Ni	750 (75)	583 (58)	301 (48)	229 (22)	5051 (558)	6109 (685)	1861 (299)	2619 (216)	4665 (1034)
Cr	0.51 (5)	0.86 (7)	1.92 (10)	0.85 (8)	17.0 (13)	18.0 (14)	16.4 (15)	17.5 (22)	17.0 (29)
Ga	4.0 (2)	3.6 (2)	4.7 (2)	2.0 (1)	64 (3)	51 (3)	40 (2)	45 (2)	72 (4)
Si	0.0014 (1)	0.0014 (6)	0.0017 (1)	0.0010 (1)	0.33 (1)	0.34 (1)	0.36 (1)	0.35 (1)	0.33 (1)
Nb	0.030 (2)	0.24 (1)	0.72 (3)	0.11 (1)	211 (21)	197 (21)	90 (10)	207 (28)	128 (15)
Ta	0.0092 (7)	0.020 (1)	0.030 (1)	0.017 (1)	10.9 (8)	10.8 (8)	5.9 (5)	11.1 (9)	9.9 (8)
Ti	<0.002	<0.002	<0.002	<0.002	0.19 (2)	0.20 (3)	0.17 (2)	0.16 (2)	0.11 (2)
Cu	20 (2)	19 (2)	11 (2)	13 (2)	86 (9)	92 (10)	49 (6)	50 (6)	92 (12)
Zn	1.14 (22)	0.39 (6)	0.36 (10)	0.76 (23)	11.9 (15)	10.2 (13)	7.8 (11)	4.7 (6)	6.2 (12)

[a] Partition coefficients for Sc, Nd, Sm, Lu, Hf, Th and U are less than 0.005 (from LA-ICPMS lower limit of detection).

[b] Values in parentheses are two standard errors of the mean in least digits cited.

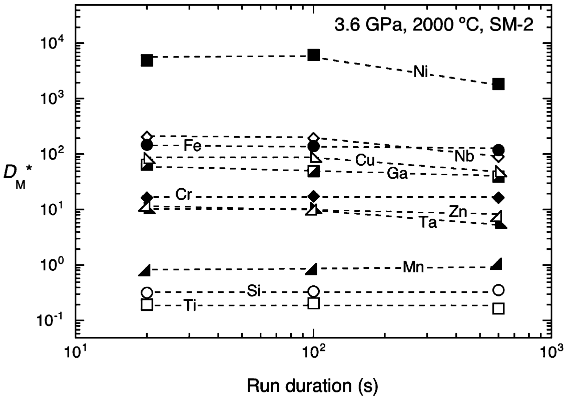

Fig. 2. Variations of molar partition coefficients (D_M*) as a function of run duration. The three experiments were performed at 3.6 GPa and 2273 K using the SM-2 composition as starting material. Error bars are within the size of symbols. Note that the partition coefficients of some elements (except Ti, Si, Cr, Fe, Mn) decrease as the run duration reaches ~600 s. As discussed in the text, this is likely due to metal infiltration in the graphite capsules.

made by Thibault and Walter (1995) on similar partitioning experiments. These authors found that runs as short as 5–300 s were sufficient to approach chemical equilibrium. In longer runs, they observed that a large portion of the metal infiltrated the C-capsule. Our time series consisted of three experiments run at 20, 100 and 600 s, respectively. The two shortest experiments did not show any significant metal infiltration as opposed to the third one. Partition coefficients for these three experiments are reported in Fig. 2. Results show that partition coefficients remain almost identical within the first 100 s of experiment. As the run duration is increased to 600 s, partition coefficients for Ni, Nb, Cu, Ga, Zn and Ta decrease by up to a factor of 2 while D^*_{Mn} increases slightly. Our observations confirm the interpretation made by Thibault and Walter (1995) that metal infiltration in the C-capsule leads to partitioning values that are not representative of equilibrium. As metal infiltration progresses, the bulk composition of the system is continuously changing, resulting in a disequilibrium between alloy and silicate. Therefore, run durations for the remaining experiments were kept short (~100 s) to minimize metal infiltration and generate partition coefficients most representative of equilibrium conditions.

3.3. Partitioning of refractory lithophile elements

One objective of this study was to test whether elements normally regarded as refractory lithophile retain their strongly lithophile behaviour at low oxygen fugacity. This is the case for Sc, Nd, Sm, Lu, Hf, Th and U, for which LA-ICPMS measurements show that their concentrations in the metal alloy are below detection limits (sub-ppm level) even under strongly reducing conditions. Corresponding partition coefficients are <0.005, an upper bound limit consistent with the absence of these elements in the core. Our result for U is in good agreement with the recent data of Wheeler et al. (2006) and Malavergne et al. (2007) who found D_U values to lie below 0.001 for S-free metal at oxygen fugacity above IW-4. In contrast to U, Th, Hf and large trivalent cations, Nb and Ta have measurable contents in the molten metal using both starting materials, with the highest contents for the more reduced composition (SM-2). Furthermore, measurable contents of Ti were detected at low oxygen fugacity. The partitioning behaviour observed for Nb, Ta and Ti is consistent with the results from previous experimental studies (e.g. Kilburn and Wood, 1997; Gessmann and Rubie, 1998; Wade and Wood, 2001; Wade and Wood, 2005). We discuss this further in the next sections.

3.4. Dependence on oxygen fugacity

Metal–silicate partitioning is known to be a function of oxygen fugacity (e.g. Schmitt et al., 1989). To understand element distribution between the core and silicate Earth during core formation, it is therefore crucial to determine the effect of oxygen fugacity on partitioning. In theory, oxygen fugacity can be calculated from the Fe and FeO content of the alloy and silicate phase, respectively (e.g. Drake et al., 1989). Relative to the iron–wüstite equilibrium, the oxygen fugacity is given by:

$$\Delta \mathrm{IW} = 2\log\left(a_{\mathrm{FeO}}^{\mathrm{silicate}}/a_{\mathrm{Fe}}^{\mathrm{metal}}\right) \quad (1)$$

where $a_{\mathrm{FeO}}^{\mathrm{silicate}}$ and $a_{\mathrm{Fe}}^{\mathrm{metal}}$ are the activities of FeO in the silicate melt and Fe in the molten metal, respectively. Activity can be calculated from activity coefficient (γ) and mole fraction (x) according to the relation $a_{\mathrm{M}}^{\mathrm{phase}} = \gamma_{\mathrm{M}}^{\mathrm{phase}} \cdot x_{\mathrm{M}}^{\mathrm{phase}}$. It follows:

$$\Delta \mathrm{IW} = 2\log\left(x_{\mathrm{FeO}}^{\mathrm{silicate}}/x_{\mathrm{Fe}}^{\mathrm{metal}}\right) + 2\log\left(\gamma_{\mathrm{FeO}}^{\mathrm{silicate}}/\gamma_{\mathrm{Fe}}^{\mathrm{metal}}\right) \quad (2)$$

As discussed later in Section 4, it is possible to calculate metal activity coefficient using the interaction parameter approach and the methodology of Ma (2001) (see Eq. (11)). The values of $\gamma_{\mathrm{Fe}}^{\mathrm{metal}}$ derived following this method cluster around 0.8, that is, tending towards small negative deviations from ideality. In contrast, published $\gamma_{\mathrm{FeO}}^{\mathrm{silicate}}$ values usually indicate positive deviations from ideal mixing behaviour. Holzheid et al. (1997) observed that $\gamma_{\mathrm{FeO}}^{\mathrm{silicate}}$ is essentially independent of temperature, oxygen fugacity and FeO content (at least to ~12 wt%) and lies around 1.7 ± 0.2. However, these authors found that $\gamma_{\mathrm{FeO}}^{\mathrm{silicate}}$ values are slightly larger with more elevated MgO contents (>20 wt%). For similar silicate liquid composition than the one of this study (~30 wt% MgO), Asahara et al. (2004) reported a ratio of FeO activity coefficient ratio between silicate liquid and magnesiowüstite of ~1.5. Combined with the value of ~2 for the activity coefficient of FeO in magnesiowüstite derived by Kilburn and Wood (1997) for MgO-rich silicate liquids, the value of $\gamma_{\mathrm{FeO}}^{\mathrm{silicate}}$ can be estimated to be close to ~3. This result is in good agreement with measurements made in MgO-rich slags in equilibrium with molten iron (Liu et al., 2001 and references therein) and with measurements by mass-spectrometry in the FeO–MgO–$\mathrm{SiO_2}$ system at high temperatures (Plante et al., 1992). Applying Eq. (2) with $\gamma_{\mathrm{FeO}}^{\mathrm{silicate}}$ and $\gamma_{\mathrm{Fe}}^{\mathrm{metal}}$ values of 3 and ~0.8, respectively, indicates that the oxygen fugacity varies between ~3.2 log units below the IW buffer (using SM-2) and ~0.8 log units below the IW buffer (using SM-1) (Table 2). These values are 0.25 log unit below or 0.35 log unit above the values that would be derived if we use $\gamma_{\mathrm{FeO}}^{\mathrm{silicate}}$ values of 4 or 2, respectively. In other words, taking the reasonable assumption that $\gamma_{\mathrm{FeO}}^{\mathrm{silicate}} = 3 \pm 1$ leads to an uncertainty in oxygen fugacity of $\pm^{0.25}_{0.35}$ log unit. Given Holzheid et al. (1997) observations, $\gamma_{\mathrm{FeO}}^{\mathrm{silicate}}$ is likely to have about the same value in all of our runs. The main variables in our experiments (FeO content (0.6–11 wt%), temperature) have been shown not to affect $\gamma_{\mathrm{FeO}}^{\mathrm{silicate}}$. This means that, even if $\gamma_{\mathrm{FeO}}^{\mathrm{silicate}}$ is not well known, the relative difference of oxygen fugacity conditions between runs performed using SM-1 and those performed using SM-2 remains approximately constant (~2.4 log unit). Finally, if we approximate activities by assuming ideal mixing behaviour (i.e. $\gamma_{\mathrm{M}}^{\mathrm{phase}} = 1$), the oxygen fugacity conditions would appear more reduced ranging between IW-4.4 and IW-2 (Table 2).

The partitioning of element M of valence v between metal and silicate can be expressed according to the equation:

$$\mathrm{M}^{\mathrm{metal}} + \frac{v}{2}\mathrm{O}_2 = \mathrm{MO}_v^{\mathrm{silicate}} \tag{3}$$

At constant pressure and temperature conditions, the following equation can be derived:

$$\log D_{\mathrm{M}}^{*} = -\frac{v}{2}\log f\mathrm{o}_2 + \log\frac{\gamma_{\mathrm{MO}_v}^{\mathrm{silicate}}}{\gamma_{\mathrm{M}}^{\mathrm{metal}}} + \mathrm{constant} \tag{4}$$

where D_{M}^{*} is the molar metal–silicate partition coefficient ($x_{\mathrm{M}}^{\mathrm{metal}}/x_{\mathrm{MO}_v}^{\mathrm{silicate}}$). Provided that the ratio of activity coefficients ($\gamma_{\mathrm{MO}_v}^{\mathrm{silicate}}/\gamma_{\mathrm{M}}^{\mathrm{metal}}$) is not a strong function of oxygen fugacity, the slope of Eq. (4) is proportional to the valence of element M in the silicate. In Fig. 3, the molar partition coefficients for experiments performed at fixed pressure and temperature (3.6 GPa 2273 K, 3.6 GPa 2473 K, 7.7 GPa 2273 K) are plotted as a function of oxygen fugacity. Given the uncertainties, the slopes obtained yield apparent valences relatively close to values expected from the literature at the low $f\mathrm{o}_2$ conditions of this study: 1+ for Cu, 2+ for Fe, Ni, Cr, Mn and Zn, 3+ for Ga, 4+ for Si and 5+ for Ta and Nb (Fig. 3). An important consequence of the dependence of D^{*}_{M} on oxygen fugacity is that a number of elements become siderophile ($D_{\mathrm{M}}^{*} > 1$) at low oxygen fugacity. For example, Nb and Zn prefer the metal to the silicate phase at conditions more reducing than about IW-1.5 (Fig. 3).

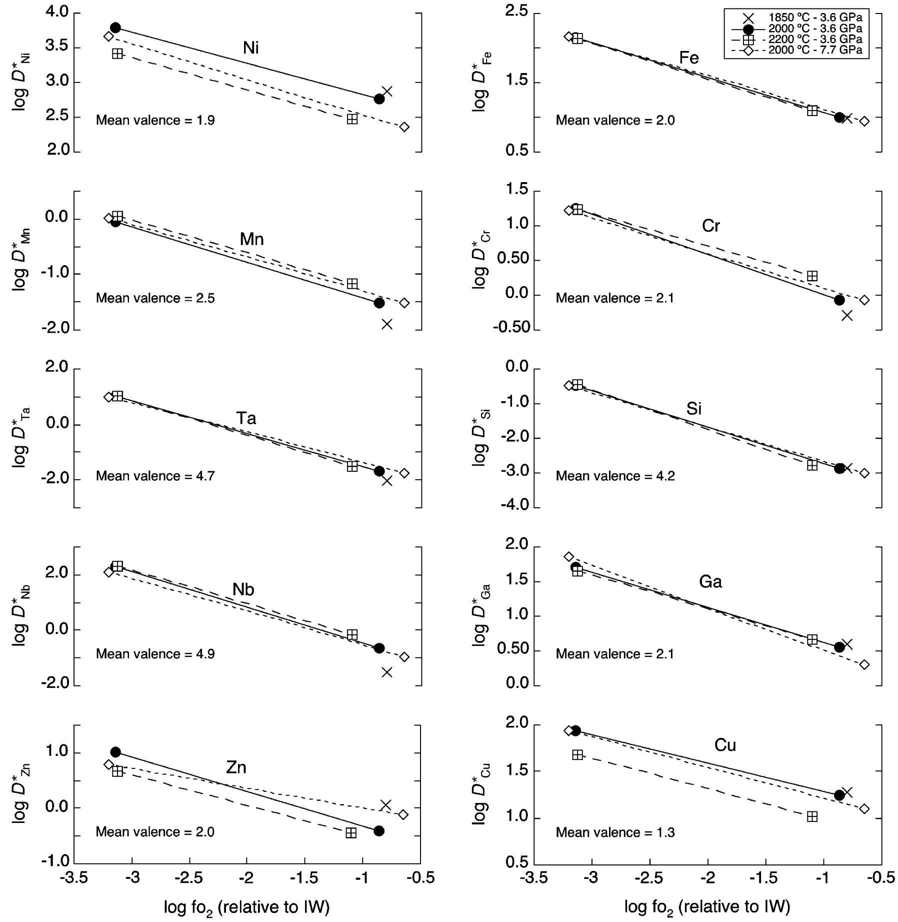

Fig. 3. Molar partition coefficients as a function of the oxygen fugacity expressed relative to the Fe–FeO (IW) buffer. See explanations in the text for the details of the calculation of oxygen fugacity. As expected from Eq. (4), all elements become more siderophile under more reducing conditions. Conditions at which elements change from preferring silicate (lithophile) to metal (siderophile) occur at log $D_{\mathrm{M}}^{*} = 0$.

3.5. Effects of pressure and temperature

Fig. 3 also allows us to have some insights into the potential effects of temperature and pressure on metal–silicate partitioning. Partition coefficients of all elements investigated except Ni are not significantly affected by an increase of pressure from 3.6 to 7.7 GPa at fixed temperature (2273 K). However, our data confirm that Ni become less siderophile at higher pressure and higher temperature, in agreement with the work of Thibault and Walter (1995) and Li and Agee (1996, 2001). An increase of temperature from 2123 to 2473 K at 3.6 GPa appears to have no significant effect on the partition coefficients of Ga, Si and Fe. Although some of the data are scattered, we find that overall D^*_{Ni}, D^*_{Zn} and D^*_{Cu} decrease with increasing temperature, while D^*_{Mn}, D^*_{Nb}, D^*_{Cr} and D^*_{Ta} increase with increasing temperature. These observations are consistent with previous results by Gessmann and Rubie (1998) and Chabot and Agee (2003) who observed that Cr and Mn become more siderophile at higher temperature with no sizeable effect of pressure. Unfortunately, Ni, Mn and Cr are the only elements among the elements of interest in this study for which the effects of pressure and temperature on partitioning have been carefully investigated. Therefore, in Section 4, we combine our data with data from the literature obtained on a wide range of pressure and temperature conditions to constrain further the relative contribution of pressure and temperature on the metal–silicate partitioning of all the elements of interest.

3.6. Compositional effects

It has been shown that metal composition, in particular its C and S contents, could affect the partitioning of a number of elements (e.g. Chabot and Agee, 2003; Wade and Wood, 2005). For example, Chabot and Agee (2003) found that the liquid metal–liquid silicate partition coefficients of V, Cr and Mn increase with increasing C content of the liquid metal, in agreement with metallurgical data (e.g. The Japan Society for the Promotion of Science and The Nineteenth Committee on Steelmaking, 1988). Thus, the larger carbon metal contents in our high fo_2 runs should favour the partitioning of elements with a chemical affinity for carbon (Mn, Cr, V, Nb, Ta and Ti according to metallurgical data). Similarly, other parameters such as the Si metal content may play a significant role and should therefore be accounted for to characterize accurately metal–silicate partitioning.

There is also experimental evidence that varying silicate composition can affect substantially metal–silicate partitioning. Although Fe, Ni, Cr and Mn are little affected, highly charged cations appear to be more sensitive to silicate melt composition (e.g. Walter and Thibault, 1995; Holzheid et al., 1997; Jana and Walker, 1997; Jaeger and Drake, 2000; O'Neill and Eggins, 2002; Chabot and Agee, 2003). As discussed by Jaeger and Drake (2000), Ga is moderately affected by a change of silicate composition, with Ga becoming less siderophile in more depolymerized melt (higher *nbo*/*t*). At present, the influence of melt composition on the partitioning of Nb, Ta, Si and Ti is not properly constrained, but dependencies similar to the ones observed for other highly charged cations are expected for these elements. The compositional variations in metal (e.g. C and Si) and silicate (e.g. Fe and Si) between our runs at low and high oxygen fugacity may generate some of the small scatter observed in terms of element valence, pressure and temperature effects discussed in the previous sections.

In the following section, we present a thermodynamic approach that allows us to take account of and correct for the effects of both silicate and metal compositions on partitioning.

4. PARAMETERIZATION

Rather than using partition coefficients to parameterize metal–silicate partitioning as done in several previous studies (e.g. Righter and Drake, 1997; Li and Agee, 2001; Chabot and Agee, 2003), we opted for a parameterization involving the molar exchange coefficient K_D^{M} similar to the one recently undertaken by Wade and Wood (2005). The advantage of using K_D^{M} rather than D^*_{M} is that when considering the former we do not need to know explicitly the oxygen fugacity. As shown hereafter, we only need to know the valence of the element of interest in the silicate melt. In contrast to previous parameterizations, Wade and Wood (2005) took explicitly into account the effect of metal composition on partitioning using metallurgical data and, using K_D^{M}, isolated the effect of oxygen fugacity from the effects of other parameters. We modified slightly their approach, as detailed below.

The partitioning of element M of valence v between metal and silicate can be described as an exchange reaction involving Fe, FeO and the oxidized and reduced components of M:

$$\underset{\text{silicate}}{\mathrm{MO}_{v/2}} + \frac{v}{2}\underset{\text{metal}}{\mathrm{Fe}} = \frac{v}{2}\underset{\text{silicate}}{\mathrm{FeO}} + \underset{\text{metal}}{\mathrm{M}} \tag{5}$$

The equilibrium constant for reaction (5) is defined as follows:

$$K_{\mathrm{a}} = \frac{\left(a_{\mathrm{FeO}}^{\mathrm{silicate}}\right)^{v/2}\cdot\left(a_{\mathrm{M}}^{\mathrm{metal}}\right)}{\left(a_{\mathrm{Fe}}^{\mathrm{metal}}\right)^{v/2}\cdot\left(a_{\mathrm{MO}_{v/2}}^{\mathrm{metal}}\right)} \tag{6}$$

Taking logarithms and rearranging using mole fractions (x) and activity coefficients (γ) yields:

$$\log K_{\mathrm{a}} = \log\left[\frac{\left(x_{\mathrm{FeO}}^{\mathrm{silicate}}\right)^{v/2}\cdot\left(x_{\mathrm{M}}^{\mathrm{metal}}\right)}{\left(x_{\mathrm{Fe}}^{\mathrm{metal}}\right)^{v/2}\cdot\left(x_{\mathrm{MO}_{v/2}}^{\mathrm{silicate}}\right)}\right] + \log\frac{\left(\gamma_{\mathrm{M}}^{\mathrm{metal}}\right)}{\left(\gamma_{\mathrm{Fe}}^{\mathrm{metal}}\right)^{v/2}} + \log\frac{\left(\gamma_{\mathrm{FeO}}^{\mathrm{silicate}}\right)^{v/2}}{\left(\gamma_{\mathrm{MO}_{v/2}}^{\mathrm{silicate}}\right)} \tag{7}$$

By definition (e.g. O'Neill, 1992), the exchange coefficient K_D^{M} is:

$$K_D^{\mathrm{M}} = \frac{\left(x_{\mathrm{FeO}}^{\mathrm{silicate}}\right)^{v/2}\cdot\left(x_{\mathrm{M}}^{\mathrm{metal}}\right)}{\left(x_{\mathrm{Fe}}^{\mathrm{metal}}\right)^{v/2}\cdot\left(x_{\mathrm{MO}_{v/2}}^{\mathrm{silicate}}\right)} = D^*_{\mathrm{M}}\cdot\left(\frac{x_{\mathrm{FeO}}^{\mathrm{silicate}}}{x_{\mathrm{Fe}}^{\mathrm{metal}}}\right)^{v/2} \tag{8}$$

It follows:

$$\log K_{\mathrm{a}} = \log K_D^{\mathrm{M}} + \log\frac{\left(\gamma_{\mathrm{M}}^{\mathrm{metal}}\right)}{\left(\gamma_{\mathrm{Fe}}^{\mathrm{metal}}\right)^{v/2}} + \log\frac{\left(\gamma_{\mathrm{FeO}}^{\mathrm{silicate}}\right)^{v/2}}{\left(\gamma_{\mathrm{MO}_{v/2}}^{\mathrm{silicate}}\right)} \tag{9}$$

Following Wade and Wood (2005), we assume that the oxide activity coefficients are not a strong function of silicate melt composition, hence that the third term remains approximately constant. From this, we expressed the apparent equilibrium constant K_{app}:

$$\begin{aligned}\log K_{\mathrm{app}} &= \log K_D^{\mathrm{M}} + \log \frac{\left(\gamma_{\mathrm{M}}^{\mathrm{metal}}\right)}{\left(\gamma_{\mathrm{Fe}}^{\mathrm{metal}}\right)^{v/2}} \\ &\approx \log K_{\mathrm{a}} + \mathrm{constant} \qquad (10)\end{aligned}$$

Like Wade and Wood (2005), we calculated metal activity coefficients using the interaction parameter approach and the method described by Ma (2001). The following equations were used:

$$\begin{aligned}\ln \gamma_{\mathrm{Fe}} = {} & \sum_{i=2}^{N} \varepsilon_i^i (x_i + \ln(1-x_i)) - \sum_{j=2}^{N-1} \sum_{k=j+1}^{N} \varepsilon_j^k x_j x_k \\ & \times \left(1 + \frac{\ln(1-x_j)}{x_j} + \frac{\ln(1-x_k)}{x_k}\right) + \sum_{i=2}^{N} \sum_{\substack{k=2 \\ (k \neq i)}}^{N} \varepsilon_i^k x_i x_k \\ & \times \left(1 + \frac{\ln(1-x_k)}{x_k} - \frac{1}{1-x_i}\right) + \frac{1}{2} \sum_{j=2}^{N-1} \sum_{k=j+1}^{N} \varepsilon_j^k x_j^2 x_k^2 \\ & \times \left(\frac{1}{1-x_j} + \frac{1}{1-x_k} - 1\right) - \sum_{i=2}^{N} \sum_{\substack{k=2 \\ (k \neq i)}}^{N} \varepsilon_i^k x_i^2 x_k^2 \\ & \times \left(\frac{1}{1-x_i} + \frac{1}{1-x_k} + \frac{x_i}{2(1-x_i)^2} - 1\right) \qquad (11)\end{aligned}$$

and

$$\begin{aligned}\ln \gamma_i = {} & \ln \gamma_{\mathrm{Fe}} + \ln \gamma_i^0 - \varepsilon_i^i \ln(1-x_i) \\ & - \sum_{j=2 (j \neq i)}^{N} \varepsilon_i^j x_j \left(1 + \frac{\ln(1-x_j)}{x_j} - \frac{1}{1-x_i}\right) \\ & + \sum_{j=2 (j \neq i)}^{N} \varepsilon_i^j x_j^2 x_i \left(\frac{1}{1-x_i} + \frac{1}{1-x_j} + \frac{x_i}{2(1-x_i)^2} - 1\right) \\ & \qquad (12)\end{aligned}$$

where γ_{Fe} and γ_i are the activity coefficients of Fe and solute i, respectively, in the molten alloy (made up of N constituents) at the temperature of interest. γ_i^0 is the activity coefficient of solute i when it is infinitely dilute in pure liquid Fe. The interaction parameters ε_i^j refer to the measured effects of component i on the activity of component j in the alloy and are dependent on the mole fraction of i (x_i) and the mole fraction of j (x_j). These parameters are tabulated in the Steelmaking Data Sourcebook (The Japan Society for the Promotion of Science and The Nineteenth Committee on Steelmaking, 1988). Since most of the ε_i^j and γ_i^0 values were obtained at the reference temperature of 1873 K ($T°$), we extrapolated them to higher temperatures using the following relationships suggested in the Steelmaking Data Sourcebook:

$$\ln \gamma_i^0(T) = \frac{T^0}{T} \ln \gamma_i^0(T^0) \qquad (13)$$

and

$$\varepsilon_i^j(T) = \frac{T^0}{T} \varepsilon_i^j(T^0) \qquad (14)$$

In the calculation of activity coefficients γ_{Fe} and γ_i, interactions between the following elements were accounted for: C, O, Si, P, S, Ti, V, Cr, Mn, Co, Ni, Ga, Ge, Zr, Nb, Mo, Hf, Ta, W, Re and Cu. When not available, the ε_i^j interaction parameter was assumed to be negligible. When not provided, the metal C content of C-bearing literature experiments was estimated by difference. Metal activity coefficients for this study calculated following the interaction parameter approach detailed here are given in Table 6 for the reader to get a better appreciation of the effects of trace element activity on partitioning. In Eq. (10), the exchange coefficients K_D^{M} were directly calculated from the metal and silicate molar compositions.

In Fig. 4, values of K_{app} calculated from equation (10) are plotted as a function of reciprocal temperature for all trace elements considered in this study. As observed by Wade and Wood (2005), we find that log K_{app} for low-pressure data from this study and the literature defined trends that parallel 1 bar free-energy data. Such agreement therefore supports the assumption of nearly constant activity coefficient ratio in silicate melts. To some extent, this observation appears to be also valid for highly charged cations, although the results are less striking due to a limited number of data.

The advantage of using exchange coefficients K_D^{M} for the parameterization rather than molar partition coefficients D_{M}^{*} is that the former is not dependent on oxygen fugacity

Table 6
Metal activity coefficients calculated using the interaction parameter approach[a]

	γ_{Fe}	γ_{Ni}	γ_{Cu}	γ_{Si}	γ_{Mn}	γ_{Cr}	γ_{Ga}	γ_{Nb}	γ_{Ta}
PL-169	0.79	0.66	6.9	0.0046	0.87	0.63	1.30	0.10	0.023
PL-185	0.82	0.69	6.1	0.0065	0.91	0.67	1.27	0.12	0.031
PR-369	0.85	0.72	5.4	0.0096	0.95	0.72	1.25	0.15	0.042
PR-373	0.72	0.63	5.8	0.0068	0.78	0.56	1.27	0.10	0.025
PR-376	0.79	0.71	8.4	0.031	0.60	0.71	0.92	0.13	1.45
PR-383	0.78	0.70	8.5	0.033	0.57	0.70	0.90	0.13	1.84
PR-375	0.76	0.70	8.6	0.034	0.56	0.69	0.90	0.12	1.98
PR-368	0.78	0.72	7.2	0.044	0.59	0.71	0.92	0.14	1.66
PR-365	0.80	0.72	8.6	0.029	0.61	0.73	0.91	0.13	1.77

[a] Because of relatively large uncertainties, γ_{Ti} and γ_{Zn} were not calculated using the interaction parameter approach.

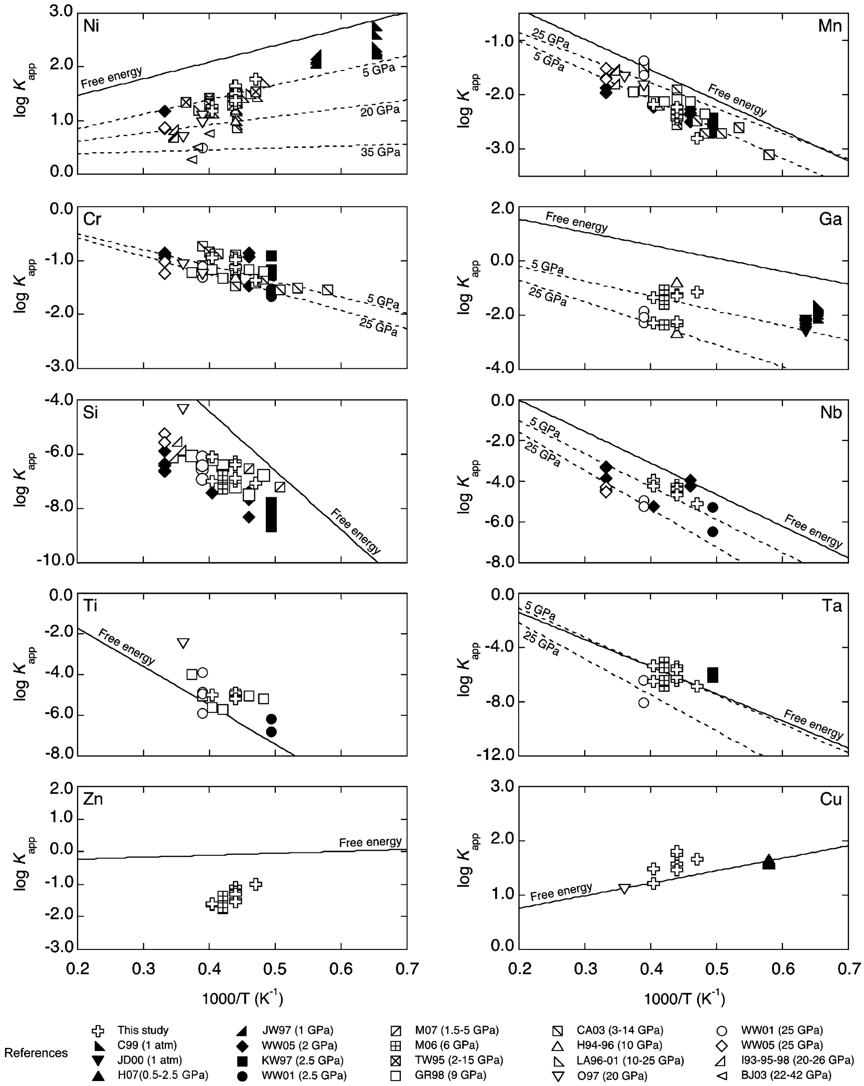

Fig. 4. Apparent equilibrium constant (K_{app}) shown as a function of reciprocal temperature ($1000/T$) for experimental runs from this study and the literature. Data were recalculated for *nbo*/*t* of 2.7 as estimated for the primitive mantle. Solid lines are 1 bar free energy data from Barin et al. (1989). Dashed lines correspond to the best-fit equation at fixed pressure and for *nbo*/*t* of 2.7. Note that there is no significant pressure effect on the metal–silicate partitioning of Si, Ti, Zn and Cu (see values of *c* coefficient and corresponding standard deviations in Table 7). References are: C99, Capobianco et al. (1993); JD00, Jaeger and Drake (2000); H07, Holzheid et al. (2007); JW97, Jana and Walker (1997); WW05, Wade and Wood (2005); KW97, Kilburn and Wood (1997); WW01, Wade and Wood (2001); M07, Malavergne et al. (2007); M06, Mann et al. (2006); TW95, Thibault and Walter (1995); GR08, Gessmann and Rubie (1998); CA03, Chabot and Agee (2003); H94-96, Hillgren et al. (1994, 1996); LA96-01, Li and Agee (1996, 2001); O97, Ohtani et al. (1997); I93-95-98, Ito et al. (1993, 1995, 1998); BJ03, Bouhifd and Jephcoat (2003).

at constant pressure and temperature (assuming a constant ratio of activity coefficients in the silicate melt). Variations in K_D^M and K_{app} should therefore reflect only the effects of pressure, temperature and composition on partitioning. To constrain the relative contribution of pressure, temperature and composition, the apparent equilibrium constant was expressed as a function of these variables using an equation of the form:

$$\log K_{app} = a + \frac{b}{T} + \frac{c \cdot P}{T} + d \cdot nbo/t \tag{15}$$

where *a*, *b*, *c* and *d* are regression constants, *T* the temperature in K, *P* the pressure in GPa, and *nbo*/*t* the molar ratio of non-bridging oxygens to tetrahedral cations in the silicate melt. By considering an equation of the form of Eq. (15), we assume that the volume change of the exchange reaction (5) is constant. In comparison to the work of Wade and Wood (2005), we added an empirical term (*nbo*/*t*) to take some account of the potential effect of silicate melt composition on partitioning of highly charged cations. As discussed by O'Neill and Eggins (2002), the use of universal melt descriptor such as *nbo*/*t* is not ideal and consideration of the activity of individual oxide components in the silicate melt should be a better way forward. However, it is not possible at present to follow this approach. Consideration of the concentration of individual oxide components rather than the *nbo*/*t* parameter does not lead to significant improvement in the parameterization (e.g. Righter and Drake, 1999). Although not a rigorous approach, we chose to keep the *nbo*/*t* term in the parameterization since it improves slightly fits to $K_{\rm app}$.

Following Wade and Wood (2005), regression coefficient *b* was estimated for all elements except Cr from 1 bar free energy data. The remaining coefficients (*a*, *c* and *d*) were obtained by linear regression. Since there are no thermodynamic data available for solid or liquid CrO, it was not possible to determine the temperature dependence of the equilibrium constant of the Fe–Cr exchange reaction. Therefore, we treated all four coefficients as unknown for the multiple linear regression of the Cr data. Furthermore, when calculating $K_{\rm app}$, we made the assumption that Cr was only present as Cr^{2+} in the silicate melt. This is likely to be the case at conditions below the IW buffer (Berry and O'Neill, 2004). Similarly, we assumed that Mn^{2+}, Ni^{2+}, Cu^{+}, Si^{4+}, Ti^{4+}, Nb^{5+}, Ta^{5+}, Ga^{3+} and Zn^{2+} were the sole species present over the range of oxygen fugacity considered in this contribution. Literature data (in agreement with this work) show that these valence states are dominant at the relatively reduced conditions investigated here. We ignored the metal activity coefficient of the trace ($\gamma^{\rm metal}_{\rm M}$) when regressing data for Zn and Ti because this term could not be calculated with sufficient precision from metallurgical data. Values of regression coefficients *a*, *b*, *c* and *d* and corresponding uncertainties are given in Table 7.

As shown in Fig. 4, temperature contributes significantly to the partitioning of a number of trace elements. Values of $K_{\rm app}$ increase (Mn, Cr, Si, Ta, Nb, Ga, Ti) or decrease (Ni, Cu, Zn) with increasing temperature, in agreement with the observations reported in Section 3.5 for molar partition coefficients. Highly charged cations (Nb, Ta, Si and Ti) are the elements with partitioning the most sensitive to variations of temperature (i.e. with largest value for *b*, Table 7). $K_{\rm app}$ values for Ni, Cr, Nb, Ta and Ga decrease with increasing pressure, while $K_{\rm app}$ for Mn increases slightly with increasing pressure. Application of the F-test shows that the pressure term (*c*) for Si, Ti, Cu and Zn is not significant at the 95% confidence level. Uncertainties on the pressure term are relatively large for these elements (Table 7). As expected from the results of O'Neill and Eggins (2002), divalent cations (Mn, Ni, Cr and Zn) do not show significant dependence on silicate composition (small *d*). We also found that the *nbo*/*t* term (*d*) was insignificant for Cu and Ti at the 95% confidence interval. From charge and size consideration, we would expect regression coefficients *b*, *c* and *d* to be similar for both Nb and Ta. This is what we obtained (with larger uncertainties for Ta). Derived regression coefficients for Mn, Si and Ni are in general agreement with those of Wade and Wood (2005). Slight differences are due to the use of a different set of data and the addition of the *nbo*/*t* term to the parameterization.

Table 7
Multiple linear regression coefficients of Eq. (15)

	n[a]	Valence[b]	*a*	*b*	*c*	*d*
Mn	71	2+	−0.02	−5600	38 (6)[c]	0.036 (10)
Ni	81	2+	0.50	3100	−78 (5)	−0.073 (15)
Cr	65	2+	0.09	−2845 (461)	−20 (10)	0.000 (13)
Ga	35	3+	3.50	−4800	−126 (36)	−0.97 (15)
Si	50	4+	2.97	−21800	−11 (33)	−0.24 (11)
Nb	21	5+	4.09	−15500	−166 (31)	−0.75 (16)
Ta	18	5+	7.74	−20000	−264 (81)	−1.69 (53)
Ti[d]	18	4+	3.46	−19000	−42 (52)	−0.11 (16)
Cu	14	1+	0.30	2300	−37 (45)	0.14 (17)
Zn[d]	13	2+	−1.11	600	−23 (102)	−0.21 (24)

[a] Number of experimental data used for the regression.

[b] Valence assumed for the regression.

[c] Values in parentheses are one standard deviation in least digits cited.

[d] Activity coefficients of Ti and Zn in the metal were not considered for the regression (see text).

5. IMPLICATIONS FOR CORE FORMATION AND CORE COMPOSITION

The parameterization allows us to model the geochemical consequences of core segregation during planetary accretion in a magma ocean. By combining Eqs. (8), (10) and (15), the molar partition coefficient of element M, $D^*_{\rm M}$, can be expressed as a function of its controlling factors (composition, oxygen fugacity, pressure and temperature):

$$\log D^*_{\rm M} = a + \frac{b}{T} + \frac{c\cdot P}{T} + d\cdot nbo/t - \frac{v}{2}\log\left(\frac{x^{\rm silicate}_{\rm FeO}}{x^{\rm metal}_{\rm Fe}}\right) - \log\frac{\left(\gamma^{\rm metal}_{\rm M}\right)}{\left(\gamma^{\rm metal}_{\rm Fe}\right)^{v/2}} \qquad (16)$$

Taking the reasonable assumption that $\gamma^{\rm metal}_{\rm Fe}$ is 1 (Raoult's Law) and rearranging for *nbo*/*t* value of 2.7 as estimated for primitive mantle composition, we obtain the following relationship:

$$\log D^*_{\rm M} = a' + \frac{b}{T} + \frac{c\cdot P}{T} - \frac{v}{2}\log\left(\frac{x^{\rm silicate}_{\rm FeO}}{x^{\rm metal}_{\rm Fe}}\right) - \log\left(\gamma^{\rm metal}_{\rm M}\right) \qquad (17)$$

where $a' = a + 2.7\cdot d$. Eq. (17) was used to calculate the evolution of elemental core-silicate Earth concentration ratio during continuous core segregation. We calculated $\gamma_{\rm M}^{\rm metal}$ at the relevant temperature using Eq. (13) and data tabulated in the Steelmaking Data Sourcebook (The Japan Society for the Promotion of Science and The Nineteenth Committee on Steelmaking, 1988). The Earth was accreted in 1% steps and the pressure of equilibration in the magma ocean was fixed at 40% of the value at the core–mantle boundary. This leads to a mean pressure of accretion of ~31 GPa. Equilibration temperatures were chosen on the peridotite liquidus, which was estimated from the data of Trønnes and Frost (2002) and Zerr et al. (1998). This leads to a mean temperature of accretion of ~2900 K. It should be mentioned that uncertainties of ±100 K on the mean temperature of accretion does not change the conclusions of this study. In our calculation, we estimated the core to constitute 32 vol% of the Earth. Results shown in Fig. 5 take account of $\pm 1\sigma$ uncertainty on the regression.

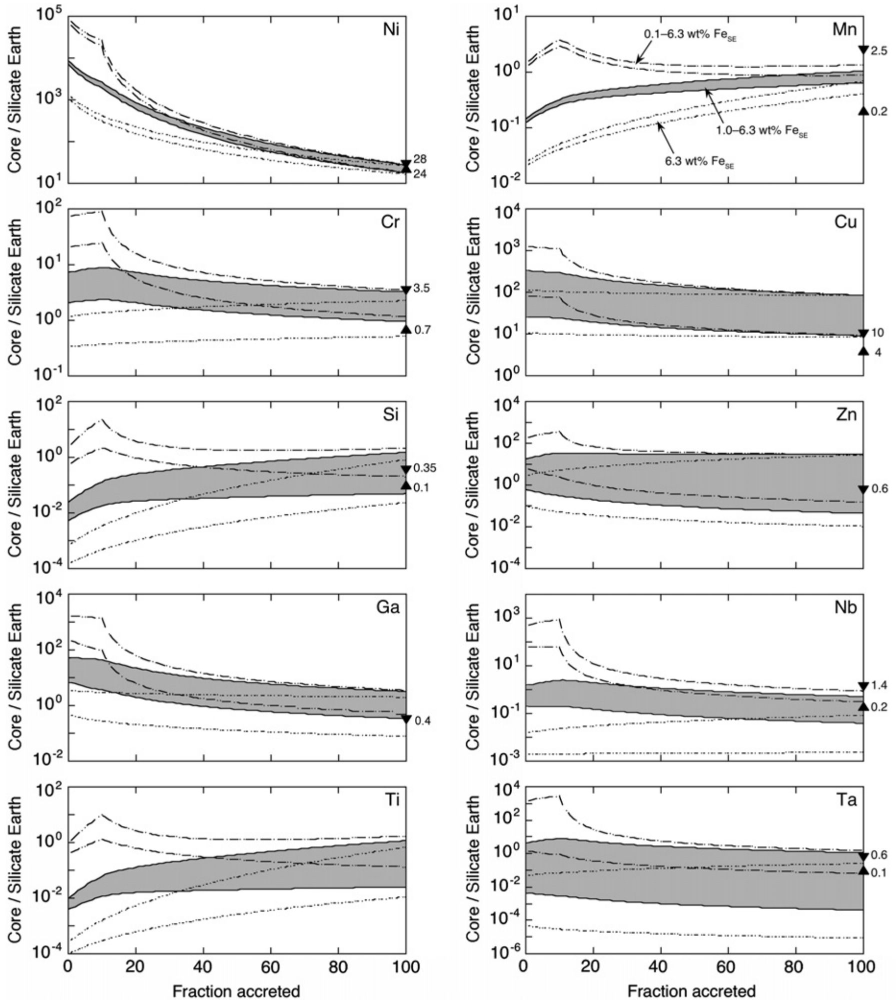

Fig. 5. Models of continuous core segregation during accretion in a deep magma ocean. Three oxygen fugacity paths are considered here using three different profiles for the Fe content of the silicate Earth (Fe$_{SE}$). For each fo_2 path, we took account of $\pm 1\sigma$ uncertainty on the regression coefficients (Table 7) to predict the range of core/silicate Earth concentration ratios. Triangles show upper (▼) and lower (▲) limits of final bulk D values required to match expected concentrations in the silicate Earth and bulk Earth. Required ranges of D values were calculated from estimates of bulk Earth and bulk silicate Earth given by Allègre et al. (1995), Allègre et al. (2001), McDonough (2003), Münker et al. (2003) and Palme and O'Neill (2003) and references therein. We find that predicted bulk D values best match required values if core formation took place under *moderately* increasing conditions of oxygen fugacity (path broadly similar to the 1.0–6.3 wt% Fe$_{SE}$ path). See discussion in text.

Three fo_2 paths were modeled by varying the Fe content of the silicate melt. In one case, the Fe content of the mantle was fixed at its current value (6.3 wt%). This means that the fo_2 is kept constant during core formation at about IW-1/-2 (depending on the value chosen for $\gamma_{\mathrm{FeO}}^{\mathrm{silicate}}$). In two additional cases, conditions become progressively oxidizing starting from fairly reduced conditions, respectively with initial Fe mantle content of 0.1 and 1.0 wt%. These contents correspond to conditions of oxygen fugacity about 4 and 2 log units below the current mantle–core equilibrium value (i.e. near IW-5/-6 and IW-3/-4, respectively). As discussed by Wade and Wood (2005), perovskite precipitation among other processes may have resulted in progressive mantle oxidation. Considering this process as the source of oxidation during accretion, oxygen fugacity was kept constant for the first 10% of accretion (since perovskite is not yet stable), and then gradually increased to reach current core–mantle equilibrium value at the end of accretion.

5.1. Nickel

The partitioning behaviour of nickel is the best constrained. Its bulk core/silicate Earth partition coefficient is also narrowly bracketed (24–28). We used this relatively tight constraint to determine a suitable depth of equilibration, hence the mean pressure and mean temperature during accretion. The appropriate equilibration depth was found to correspond to $40 \pm 5\%$ of the depth of the core–mantle boundary. It should be noted that this value is independent of the conditions of oxygen fugacity. Furthermore, variation of the relative depth of the magma ocean within the $40 \pm 5\%$ range does not affect the conclusions reached below.

5.2. Chromium, copper, manganese and silicon

As shown in Fig. 5, the bulk core-silicate Earth partition coefficients we predict for Mn, Cr, Si and Cu are all in agreement with expected values whatever the fo_2 path that is considered. Although not shown here, it is important to mention that similar conclusions can be reached for Cr whether we assume a valence of 2+ or 3+. It is interesting to note that derived D_{Mn} values for the three fo_2 paths range between 0.4 and 1.4, as opposed to the 0.2–2.5 range derived from the bulk Earth (800–1390 ppm) and silicate Earth (1045–1160 ppm) estimates of Allègre et al. (2001), Palme and O'Neill (2003) and McDonough (2003). Since it is likely that fo_2 conditions envisaged here encompass the actual conditions during core formation, we can constrain further the Mn budget of the planet. Assuming that the silicate Earth contains 1100 ppm of Mn, we derive a core Mn content of 440–1540 ppm and a bulk Earth Mn content of 890–1240 ppm. The range of modeled bulk D_{Cu} lies between 8 and 85 and is almost independent of the chosen fo_2 path. This compares to expected D_{Cu} between 4 and 10. Our modeling, which predicts relatively high core/silicate Earth ratio for Cu (8–10), is this consistent with the low silicate Earth estimate (~20 ppm) of Palme and O'Neill (2003) (as opposed to ~30 ppm estimated by McDonough, 2003). A bulk D_{Cu} of 8–10 would lead to a core Cu content of ~160 ppm, i.e. ~25% more than proposed by McDonough (2003).

5.3. Niobium and tantalum

The Nb and Ta budget of the silicate Earth has been the subject of considerable debate in recent years (e.g. McDonough, 1991; Rudnick et al., 2000; Wade and Wood, 2001; Münker et al., 2003; Schmidt et al., 2004). It has been shown that all the major reservoirs of the silicate Earth display subchondritic Nb/Ta ratios (e.g. Rudnick et al., 2000; Münker et al., 2003), with recent estimates for the bulk silicate Earth between 14 and 14.7, as opposed to 17.4 and 19.9 for the bulk Earth (Münker et al., 2003; Palme and O'Neill, 2003). Mass balance considerations therefore require an unsampled reservoir with superchondritic Nb/Ta. It has been suggested that subducted oceanic crust in the lower mantle could be the missing reservoir (Kamber and Collerson, 2000; Rudnick et al., 2000), and hence, the bulk silicate Earth Nb/Ta ratio may therefore be chondritic as recently put forward by McDonough (2003). However, a recent experimental study (Schmidt et al., 2004) concluded that the superchondritic Nb/Ta ratio of subducted oceanic crust would be too low and would require an unrealistically large volume of basaltic crust to balance the remaining subchondritic reservoirs of the silicate Earth. Münker et al. (2003) also suggested that this reservoir was unlikely to be significant since HIMU ocean island basalts, which should tap this reservoir, have subchondritic Nb/Ta ratios (~16). As an alternative, it has been suggested that the silicate Earth has subchondritic Nb/Ta ratio as a consequence of preferential extraction of Nb relative to Ta into the core. Wade and Wood (2001) provided experimental arguments in favour of this hypothesis. Using the Nb/Ta ratios determined by Münker et al. (2003) for the silicate Earth and the bulk Earth and taking account of the corresponding uncertainties, bulk D_{Nb} and D_{Ta} should lie within 0.5–1.4 and 0.2–0.6, respectively. Less extreme values from Palme and O'Neill (2003) lead to a range of 0.2–0.7 for D_{Nb} and a range of 0.1–0.4 for D_{Ta}.

For core formation at constant oxygen fugacity (6.3 wt% Fe in the mantle), our predicted upper limit for D_{Nb} is 0.09, which is below the expected range (0.2–1.4) from the data of Münker et al. (2003) and Palme and O'Neill (2003). With 6.3 wt% Fe in the primitive mantle, we predict an upper limit for D_{Ta} (0.26) that falls within the expected range (0.1–0.6). However, if we assume that the core has a superchondritic Nb/Ta ratio between 23 and 32 as required to balance the bulk Earth and bulk silicate Earth (Münker et al., 2003; Palme and O'Neill, 2003), D_{Ta} should be lower than 0.05, i.e. below the expected range. In contrast to the path at constant fo_2, paths with progressively increasing oxygen fugacity (from 0.1/1.0 to 6.3 wt% Fe) lead to Nb and Ta concentrations in the core and mantle that are consistent with expected values (Fig. 5). Therefore, these predictions for Nb and Ta allow exclusively a scenario of core formation under relatively reduced initial conditions, not under constant oxygen fugacity near IW-1/-2. Given the dependence of Nb and Ta partitioning on temperature, the latter would require equilibrium temperatures during accretion that are well in excess of the estimated peridotite liquidus, which is physically impossible.

5.4. Gallium

Ga plots almost directly on the volatility trend defined by the most lithophile volatile elements like Li, Na and Rb (see Fig. 6 of McDonough, 2003). In comparison with Na, which has almost the same condensation temperature (Wasson, 1985; Lodders, 2003), Ga has a BSE/CI-chondrite normalized ratio that is about 10–20% (±10%) lower (McDonough and Sun, 1995; McDonough, 2003; Palme and O'Neill, 2003). This implies that a minor fraction of the Ga budget (0–30%) is in the core and that Ga depletion in the silicate Earth relative to chondrite is mostly due to loss by volatilization prior to accretion. For the upper bound of 30% Ga in the core, the corresponding D_{Ga} is 0.43. Our results suggest that the lowest fo_2 path considered here (0.1–6.3 wt% Fe) leads to bulk D_{Ga} values (0.53–3.5) higher than the expected range (0–0.4). The other two fo_2 paths can reproduce adequately the expected range of bulk D_{Ga} with the best fit being obtained at constant fo_2 (0.1–2). The intermediate fo_2 path leads to larger D_{Ga} between 0.34 and 3.2, which overlap slightly the expected range (Fig. 5).

5.5. Zinc

Zn also plots on the volatility trend, but a direct comparison with fluorine (F), which has essentially the same condensation temperature, is out of place given the uncertainty on the silicate Earth content of F (15–25 ppm; McDonough, 2003; Palme and O'Neill, 2003). Zn content is much better constrained in the silicate Earth (~55 ppm;

McDonough, 2003; Palme and O'Neill, 2003) than it is in the bulk Earth. McDonough (2003) derived a content of ~40 ppm for the bulk Earth, based on the assumption that Zn is not present in the core. Allègre et al. (2001) estimated the Earth to contain 24 ± 2 ppm of Zn. If correct, this latter value would imply that the silicate Earth content of 55 ppm is overestimated. Considering the silicate Earth content from McDonough (2003) and Palme and O'Neill (2003) as appropriate and taking account of uncertainties, one can envisage that the core may contain up to ~30 ppm of Zn. This corresponds to an upper limit of 0.6 for D_{Zn}. As shown in Fig. 5, a range of D_{Zn} between 0 and 0.6 can be matched within uncertainty by the three $f\mathrm{o}_2$ paths considered here.

5.6. Titanium

Ti is normally regarded as a refractory lithophile element. Hence, the core is not expected to contain any significant amount of Ti. Our predictions remain relatively tentative at present owing to large uncertainties on the effect of pressure and composition (Table 7). The sole conclusion that can be reached is that for core formation under $f\mathrm{o}_2$ conditions of the current core–mantle equilibrium (6.3 wt% Fe) shows that D_{Ti} should be at least 0.01 (Fig. 5). This compares with a minimum D_{Ti} of 0.025 for the 0.1–6.3 wt% Fe path. In other words, the core should contain at least 0.5% of the Earth's Ti (>13 ppm).

6. SUMMARY AND CONCLUSIONS

In summary, it is possible to fit the predicted D values from our model with the expected values for Ni, Mn, Cr, Si, Nb, Ta, Cu, Zn and Ga provided that core segregation took place under oxidizing conditions starting from moderately reduced and finishing at the current mantle–core equilibrium value. Although not shown here, such conditions would be also consistent with the silicate Earth depletions in V, Co, P and W using the parameterization given by Wade and Wood (2005). We show, that if initial $f\mathrm{o}_2$ conditions were highly reducing (for example for 0.1–6.3 wt% Fe), the silicate Earth depletion in Ga would be more pronounced than observed. Conversely, if $f\mathrm{o}_2$ conditions were kept relatively oxidized near the current core–mantle equilibrium value, Nb and Ta contents in the silicate Earth would exceed the observed values. Using a more complete set of elements, we confirm the conclusions reached by Wade and Wood (2005) that oxygen fugacity should have increased during accretion. Finally, our results suggest that in addition to volatilization, core formation would contribute to the depletion of Ga, Cr, Mn and Zn in the silicate Earth.

As shown by the conclusions reached in this contribution, the new way of parameterizing partitioning data initiated by Wade and Wood (2005) and further developed here is a potentially powerful tool to understand the geochemical implications of core formation in a magma ocean. Additional high-pressure and high-temperature experiments are needed to improve the present parameterization, particularly for Si, Ga, Ta, Ti, Cu and Zn for which uncertainties are the largest. In addition to refine our understanding of core formation, these new data will eventually help quantify the trace element composition of the core and place tighter constraints on the light element budget of the core.

ACKNOWLEDGMENTS

We thank Ute Mann and Astrid Holzheid for permitting us to use their preliminary experimental data, and Nachiketa Rai for discussions. We are also grateful to Richard Ash, Suzy Elhlou, Chris Hadidiacos and Norman Pearson for technical assistance. We thank Julien Siebert, Michael Walter and an anonymous reviewer for comments that helped clarify the manuscript. The Carnegie Institution of Washington (Postdoctoral Fellowships to A.C. and S.K.), the NASA (Cosmochemistry Grant NNG04GG09G to YF) and the NSF (Grant EAR0337621 to W.F.M.) supported this work. Research at Macquarie University is supported by ARC grants FF0456999 and DP066453 to B.J.W. Funding for the GEMOC LA-ICPMS and EPMA probes comes from ARC LIEF and DEST Systemic Infrastructure Grants, Macquarie University and industry. This is contribution No. 495 from the ARC GEMOC National Key Centre (www.es.mq.edu.au/GEMOC).

REFERENCES

Allègre C. J., Poirier J.-P., Humler E. and Hofmann A. W. (1995) The chemical composition of the Earth. *Earth Planet. Sci. Lett.* **134**, 515–526.

Allègre C., Manhès G. and Lewin E. (2001) Chemical composition of the Earth and the volatility control on planetary genetics. *Earth Planet. Sci. Lett.* **185**, 49–69.

Asahara Y., Kubo T. and Kondo T. (2004) Phase relations of a carbonaceous chondrite at lower mantle conditions. *Phys. Earth Planet. Inter.* **143-144**, 421–432.

Barin I., Sauert F., Schultze-Rhonhof E. and Sheng W. S. (1989) *Thermochemical Data of Pure Substances, Part I and Part II.* CH Verlagsgesellschaft, Weinheim, Germany.

Berry A. J. and O'Neill H. S. C. (2004) A XANES determination of the oxidation state of chromium in silicate glasses. *Am. Mineral.* **89**, 790–798.

Bouhifd M. A. and Jephcoat A. P. (2003) The effect of pressure on partitioning of Ni and Co between silicate and iron-rich metal liquids: a diamond-anvil cell study. *Earth Planet. Sci. Lett.* **209**, 245–255.

Capobianco C. J., Jones J. H. and Drake M. J. (1993) Metal–silicate thermochemistry at high temperature: magma oceans and the excess siderophile element" problem of the Earth's upper mantle. *J. Geophys. Res.* **98**, 5433–5443.

Chabot N. L. and Agee C. B. (2003) Core formation in the Earth and Moon: new experimental constraints from V, Cr, and Mn. *Geochim. Cosmochim. Acta* **67**, 2077–2091.

Corgne A., Keshav S., McDonough W. F. and Fei Y. (2007) How much potassium is in the core? New insights from partitioning experiments. *Earth Planet. Sci. Lett.* **256**, 567–576.

Cottrell E. and Walker D. (2006) Constraints on core formation from Pt partitioning in mafic silicate liquids at high temperatures. *Geochim. Cosmochim. Acta* **70**, 1565–1580.

Danielson, L., Sharp, T. and Hervig, R. L. (2005) Implications for core formation of the Earth from high pressure-temperature Au partitioning experiments. Lunar and Planetary Science Conference XXXVI, Lunar Planet. Inst., Houston. #1955 (abstr.).

Drake M. J., Newsom H. E. and Capobianco C. J. (1989) V, Cr and Mn in the Earth, Moon, EPB, and SPB and the origin of the Moon: Experimental studies. *Geochim. Cosmochim. Acta* **53**, 2101–2111.

Ertel W., Walter M. J., Drake M. J. and Sylvester P. J. (2006) Experimental study of platinum solubility in silicate melt to 14 GPa and 2273 K: Implications for accretion and core formation in Earth. *Geochim. Cosmochim. Acta* **70**, 2591–2602.

Gessmann C. K. and Rubie D. C. (1998) The effect of temperature on the partitioning of nickel, cobalt, manganese, chromium, and vanadium at 9 GPa and constraints on formation of the Earth's core. *Geochim. Cosmochim. Acta* **62**, 867–882.

Hillgren V. J., Drake M. J. and Rubie D. C. (1994) High-pressure and high-temperature experiments on core–mantle segregation in the accreting Earth. *Science* **264**, 1442–1445.

Hillgren V. J., Drake M. J. and Rubie D. C. (1996) High pressure and high temperature metal–silicate partitioning of siderophile elements: the importance of silicate liquid composition. *Geochim. Cosmochim. Acta* **60**, 2257–2263.

Holzheid A., Palme H. and Chakraborty S. (1997) The activities of NiO, CoO and FeO in silicate melts. *Chem. Geol.* **139**, 21–38.

Holzheid A., Sylvester P., O'Neill H. S. C., Rubie D. C. and Palme H. (2000) Evidence for a late chondritic veneer in the Earth's mantle from high-pressure partitioning of palladium and platinum. *Nature* **406**, 396–399.

Holzheid A., Kegler Ph., Frost D., Rubie D.C. and Palme H. (2007) Partitioning behaviour of Copper and Germanium: implications for terrestrial core formation scenarios. Lunar and Planetary Science Conference XXXVIII, Lunar Planet. Inst., Houston. #2090 (abstr.).

Ito E., Katsura T. and Suzuki T. (1998) Metal/silicate partitioning of Mn, Co, and Ni at high-pressures and high temperatures and implications for core formation in a deep magma ocean. In *Properties of Earth and Planetary Materials at High Pressure and Temperature* (ed. M. H. Manghnani), pp. 215–225. Geophysical Monograph 101. American Geophysical Union.

Ito E., Morooka K. and Ujike O. (1993) Dissolution of K in molten iron at high pressure and temperature. *Geophys. Res. Lett.* **20**, 1651–1654.

Ito E., Morooka K., Ujike O. and Katsura T. (1995) Reaction between molten iron and silicate melts at high pressure: Implications for the chemical evolution of the Earth's core. *J. Geophys. Res.* **100**, 5901–5910.

Jaeger W. L. and Drake M. J. (2000) Metal–silicate partitioning of Co, Ga, and W: dependence on silicate melt composition. *Geochim. Cosmochim. Acta* **64**, 3887–3895.

Jana D. and Walker D. (1997) The influence of silicate melt composition on distribution of siderophile elements among metal and silicate liquids. *Earth Planet. Sci. Lett.* **150**, 463–472.

Kamber B. S. and Collerson K. D. (2000) Role of 'hidden' deeply subducted slabs in mantle depletion. *Chem. Geol.* **166**, 241–254.

Kilburn M. R. and Wood B. J. (1997) Metal–silicate partitioning and the incompatibility of S and Si during core formation. *Earth Planet. Sci. Lett.* **152**, 139–148.

Li J. and Agee C. B. (1996) Geochemistry of core–mantle differentiation at high pressure. *Nature* **381**, 686–689.

Li J. and Agee C. B. (2001) The effect of pressure, temperature, oxygen fugacity and composition on partitioning of nickel and cobalt between liquid Fe–Ni–S alloy and liquid silicate: implications for the earth's core formation. *Geochim. Cosmochim. Acta* **65**, 1821–1832.

Liu S.-H., Fruehan R. J., Morales A. and Ozturk B. (2001) Measurement of FeO activity and solubility of MgO in smelting slags. *Metall. Mater. Trans. B* **32**, 31–36.

Lodders K. (2003) Solar system abundances and condensation temperatures of the elements. *Astrophys. J.* **591**, 1220–1247.

Ma Z. (2001) Thermodynamic description for concentrated metallic solutions using interaction parameters. *Metall. Mater. Trans. B* **32**, 87–103.

Malavergne V., Tarrida M., Combes R., Bureau H., Jones J. and Schwandt C. (2007) New high-pressure and high-temperature metal/silicate partitioning of U and Pb: Implications for the cores of the Earth and Mars. *Geochim. Cosmochim. Acta* **71**, 2637–2655.

Mann, U., Frost, D. J., Rubie, D. C., Shearer, C. K. and Agee, C.B. (2006) Is silicon a light component in the Earth's core? Constraints from liquid metal–liquid silicate partitioning of some lithophile elements. Lunar and Planetary Science Conference XXXVII, Lunar Planet. Inst., Houston. #1161 (abstr.).

McDonough W. F. (1991) Partial melting of subducted oceanic crust and isolation of its residual eclogitic lithology. *Phil. Trans. R. Soc. A* **335**, 407–418.

McDonough, W. F. (2003) Compositional model for the Earth's core. In: (ed. R.W. Carlson) The Mantle and Core, Treatise on Geochemistry, vol. 2 (eds. H. Holland and K.K. Turekian). Elsevier–Pergamon, Oxford. pp. 547–568.

McDonough W. F. and Sun S.-S. (1995) The composition of the Earth. *Chem. Geol.* **120**, 223–253.

Münker C., Pfänder J. A., Weyer S., Büchl A., Kleine T. and Mezger K. (2003) Evolution of planetary cores and the Earth–Moon system from Nb/Ta systematics. *Science* **301**, 84–87.

O'Neill H. S. C. (1991) The origin of the moon and the early history of the earth–A chemical model. Part 2: the earth. *Geochim. Cosmochim. Acta* **55**, 1159–1172.

O'Neill H. S. C. (1992) Siderophile elements and the Earth's formation. *Science* **257**, 1281–1285.

O'Neill H. S. C. and Eggins S. M. (2002) The effect of melt composition on trace element partitioning: an experimental investigation of the activity coefficients of FeO, NiO, CoO, MoO_2 and MoO_3 in silicate melts. *Chem. Geol.* **186**, 151–181.

Ohtani E., Yurimoto H. and Seto S. (1997) Element partitioning between metallic liquid, silicate liquid, and lower-mantle minerals: implications for core formation of the Earth. *Phys. Earth Planet. Inter.* **100**, 97–114.

Palme, H. and O'Neill, H. S. C. (2003) Cosmochemical estimates of mantle composition. In The Mantle and Core (ed. R.W. Carlson), Treatise on Geochemistry, vol. 2 (eds. H. Holland and K. K. Turekian). Elsevier–Pergamon, Oxford. pp. 1–38.

Plante E. R., Hastie J. W. and Kowalska M. (1992) Activity of FeO in the FeO–MgO–SiO_2 system determined by high temperature mass spectrometry. *ISIJ International* **32**, 1276–1279.

Righter K. and Drake M. J. (1997) Metal–silicate equilibrium in a homogeously accreting earth: new results for Re. *Earth Planet. Sci. Lett.* **146**, 541–553.

Righter K. and Drake M. J. (1999) Effect of water on metal–silicate partitioning of siderophile elements: a high pressure and temperature terrestrial magma ocean and core formation. *Earth Planet. Sci. Lett.* **171**, 383–399.

Rudnick R. L., Barth M., Horn I. and McDonough W. F. (2000) Rutile-bearing refractory eclogites: missing link between continents and depleted mantle. *Science* **287**, 278–281.

Schmidt M. W., Dardon A., Chazot G. and Vannucci R. (2004) The dependence of Nb and Ta rutile-melt partitioning on melt composition and Nb/Ta fractionation during subduction processes. *Earth Planet. Sci. Lett.* **226**, 415–432.

Schmitt W., Palme H. and Wänke H. (1989) Experimental determination of metal/silicate partition coefficients for P, Co, Ni, Cu, Ga, Ge, Mo, and W some implications for the early evolution of the Earth. *Geochim. Cosmochim. Acta* **53**, 173–185.

The Japan Society for the Promotion of Science and The Nineteenth Committee on Steelmaking (1988) Part 2: Recommended values of activity and activity coefficients, and interaction parameters of elements in iron alloys. In Steelmaking

Data Sourcebook. Gordon and Breach Science Publishers, New York. pp. 273–297.

Thibault Y. and Walter M. J. (1995) The influence of pressure and temperature on the metal–silicate partition coefficients of nickel and cobalt in a model C1 chondrite and implications for metal segregation in a deep magma ocean. *Geochim. Cosmochim. Acta* **59**, 991–1002.

Trønnes R. G. and Frost D. J. (2002) Peridotite melting and mineral-melt partitioning of major and minor elements at 22–24.5 GPa. *Earth Planet. Sci. Lett.* **197**, 117–131.

Wade J. and Wood B. J. (2001) The Earth's 'missing' niobium may be in the core. *Nature* **409**, 75–78.

Wade J. and Wood B. J. (2005) Core formation and the oxidation state of the Earth. *Earth Planet. Sci. Lett.* **236**, 78–95.

Walker D., Norby L. and Jones J. H. (1993) Superheating effects on metal–silicate partitioning of siderophile elements. *Science* **262**, 1858–1861.

Walter M. J., Newsom H. E., Ertel W. and Holzheid A. (2000) Siderophile elements in the Earth and Moon: metal–silicate partitioning and implications for core formation. In *Origin of the Earth and Moon* (eds. R. M. Canup and K. Righter). University of Arizona Press, Tucson, pp. 265–289.

Walter M. J. and Thibault Y. (1995) Partitioning of tungsten and molybdenum between metallic liquid and silicate melt. *Science* **270**, 1186–1189.

Wanke H. (1981) Constitution of the terrestrial planets. *Phil. Trans. R. Soc. A* **303**, 287–302.

Wasson J. T. (1985) *Meteorites: Their Record of Early Solar-system History*. W.H. Freeman and Company, New York.

Wasson J. T. and Kallemeyn G. W. (1988) Compositions of chondrites. *Phil. Trans. R. Soc. A* **325**, 535–544.

Wheeler K. T., Walker D., Fei Y., Minarik W. G. and McDonough W. F. (2006) Experimental partitioning of uranium between liquid iron sulfide and liquid silicate: Implications for radioactivity in the Earth's core. *Geochim. Cosmochim. Acta* **70**, 1537–1547.

Zerr A., Diegeler A. and Boehler R. (1998) Solidus of the Earth's deep mantle. *Science* **281**, 243–246.

Associate editor: F.J. Ryerson